

Pre-Print Copy: Garlock et al. (2019). "Post-buckling mechanics of a square slender steel plate in pure shear." *Engineering Journal (AISC)*, Vol. 56, No. 1, pp. 27-46.

21 simply-supported plate with an aspect ratio equal to 1.0 and slenderness ratio equal to 134.
22 Results show that localized bending in the plates due to the out-of-plane post-buckling
23 deformations appear to be a significant factor in the ultimate shear post-buckling capacity
24 of the plate. Also, the compressive stresses continue to increase beyond the onset of elastic
25 buckling in some regions of the plate, contrary to current design assumptions. Overall, this
26 study provides new insights into the mechanics of shear post-buckling behavior of thin
27 plates that can be exploited for design procedures that are consistent with mechanical
28 behavior.

29 **Keywords:** Shear, Buckling, Tension Field, Slender Plates, Web, Plate Girder

30

31 **1. Introduction**

32 Deep steel beams (i.e., plate girders) have thin webs and are commonly used in steel
33 construction for buildings but most notably in bridges. The design of these elements is
34 often controlled by the shear strength of the slender web plate. Web plates that elastically
35 buckle due to shear load still possess a significant amount of post-buckling shear strength.
36 Post-buckling capacity is utilized in the design of many bridge girders due to high web
37 slenderness, which is necessitated by large girder depths and weight/material savings.
38 This post-buckling behavior has attracted the attention of researchers and engineers since
39 the 1880s (e.g., Basler, 1961; Wagner 1931; Wilson 1886). Since 1931, more than a dozen
40 proposals have been developed to explain and predict the post-buckling shear strength of
41 thin webs in plate girders (e.g., Höglund, 1997; Porter et al., 1975). A detailed discussion of
42 the differences between several of the aforementioned proposals is provided by White and
43 Barker (2008). Despite these numerous proposals, the true mechanics and post-buckling

Pre-Print Copy: Garlock et al. (2019). "Post-buckling mechanics of a square slender steel plate in pure shear." *Engineering Journal (AISC)*, Vol. 56, No. 1, pp. 27-46.

44 behavior are still not fully understood, particularly the contributions of the compression
45 field and vertical stiffeners to the ultimate post-buckling shear strength. Previous
46 publications have provided extensive discussions on the various proposed plate shear
47 buckling models throughout the literature (Ziemian, 2010; White & Barker, 2008; Yoo &
48 Lee, 2006), and all the models are based on *tension field action*. Tension field theory posits
49 that the main source of this post-buckling shear strength is the development of tensile
50 stresses in a defined diagonal field, which is mobilized after the onset of elastic shear
51 buckling. Recent research, however, has shown that the fundamental assumptions upon
52 which tension field action is based do not represent the full mechanical response of web
53 shear buckling (Yoo & Lee, 2006; Glassman & Garlock, 2016; Jha 2016).

54
55 In addition, the current AISC Specification (2016) recognizes that the vertical stiffener does
56 not carry the full vertical component of the tension field force. In previous editions, this
57 stiffener was designed for an area consistent with the assumed vertical component of the
58 tension field force, whereas it is currently designed for flexural stiffness only. This change
59 rightly recognizes that the vertical stiffener provides lateral stiffness to define the web
60 panelization – it does not act as an anchor for the tension field. As noted in the AISC
61 Specification's commentary: "...transverse stiffeners in I-girders designed for shear post-
62 buckling strength, including tension field action, are loaded predominantly in bending due
63 to the restraint they provide to lateral deflection of the web. Generally, there is evidence of
64 some axial compression in the transverse stiffeners due to the tension field, but even in the
65 most slender web plates permitted by this Specification, the effect of the axial compression
66 transmitted from the post-buckled web plate is typically minor compared to the lateral

Pre-Print Copy: Garlock et al. (2019). "Post-buckling mechanics of a square slender steel plate in pure shear." *Engineering Journal (AISC)*, Vol. 56, No. 1, pp. 27-46.

67 loading effect. Therefore, the transverse stiffener area requirement from prior AISC
68 Specifications is no longer specified." (AISC 2016). However, the design equations that
69 predict the post-buckling capacity are still based on the original tension field design
70 procedures. Using the current approach, the load path for the tension field action is,
71 therefore, incomplete - the vertical component of the diagonal tension field must be
72 resolved via a different mechanism. The study presented in this paper provides, for the
73 first time, insights to the behavior of thin web plates that, with more investigation, can lead
74 to updated design recommendations that include a completed load path.

75
76 This paper explores the fundamental behavior of thin plates under pure shear. Using
77 validated finite element analyses, outputs such as plastic strains, von Mises stresses,
78 principal stresses, and principal stress directions are examined on the buckled plate. The
79 through-thickness bending and membrane stresses in the plate elements are also
80 evaluated. These evaluations are performed for a plate with an aspect ratio equal to 1.0 and
81 slenderness ratio equal to 134. Examining this single case provides novel insights into
82 plate shear buckling behavior that will be used as a basis for future work, which will
83 examine a wider range of plate parameters.

84

85 **2. Finite Element Model**

86 The plate used for this study is based on standard plans for typical steel girder highway
87 bridges specified by the Federal Highway Administration (FHWA, 1982). A 90 foot (27.4-
88 meter) span design was used as a prototype, where the depth, D , equals 58 inches (1473
89 mm), and the web thickness, t_w , equals 7/16 inches (11 mm). In practice, many of these

Pre-Print Copy: Garlock et al. (2019). "Post-buckling mechanics of a square slender steel plate in pure shear." *Engineering Journal (AISC)*, Vol. 56, No. 1, pp. 27-46.

90 girders are designed with a transverse stiffener spacing, a , greater than D ; however, in this
91 study we assume $a = D$. Future work will examine other stiffener spacings. The steel was
92 modeled with a yield stress equal to 50 ksi (345 MPa), a modulus of elasticity equal to
93 29,000 ksi (200 GPa), and Poisson's ratio equal to 0.3. It will be shown that the steel
94 remained in the elastoplastic region for the range of strains encountered in the analyses
95 (well before strain-hardening occurs).

96
97 The finite element (FE) model was developed in the software Abaqus (Dassault Systemes
98 2011) using the simply-supported boundary conditions shown in Fig. 1. Note that the
99 boundary conditions used here represent an approximation of the actual boundary
100 conditions which may incorporate flanges and stiffeners, each of varying stiffnesses. To
101 achieve perfectly symmetric stress results, the boundary conditions used by the authors
102 differ only slightly from those used by Glassman and Garlock (2016), which restrained the
103 Y-translation on the left side instead of applying a load. The elastic critical shear buckling
104 load, V_{cr} , and the ultimate post-buckling shear load, V_u , are not affected by this slight
105 modification in boundary condition.

106
107 Yoo and Lee (2006) used boundary conditions that were different from both configurations
108 mentioned above. In their studies, the z-direction translation is free on all four sides. Such
109 a boundary condition represents a lower-bound solution for V_u . The current study's
110 boundary conditions assume axially rigid flanges and are thus closer to an upper-bound
111 solution. All boundary conditions discussed here result in the same V_{cr} . Comparing V_u
112 using the Yoo and Lee (2006) boundary conditions to that produced by the current study's

Pre-Print Copy: Garlock et al. (2019). "Post-buckling mechanics of a square slender steel plate in pure shear." *Engineering Journal (AISC)*, Vol. 56, No. 1, pp. 27-46.

113 boundary conditions (Fig. 1), one obtains V_u values equal to 437 kips and 593 kips,
 114 respectively, when analyzing the prototype plate. The current study's results match those
 115 of Glassman and Garlock (2016), which correlated well to experimental results (as will be
 116 discussed later in this paper). The authors, therefore, proceed with the boundary
 117 conditions of Fig. 1 for the remainder of this paper.

118

119 The thin plate was meshed using S4 shell elements (doubly curved, general-purpose, finite
 120 membrane strains) with 4 integration points on the surface as shown in Fig. 2. A
 121 preliminary study was conducted to determine an appropriate number of section points
 122 through the depth, in which 3, 5, 7, and 9 section points at each surface integration point
 123 were evaluated by examining stress values and shear load sustained at $V = V_u$. The results
 124 for 5, 7, and 9 section points differed by less than 1%, and 5 section points as shown in Fig.
 125 2 are therefore used for all other analyses discussed in this paper.

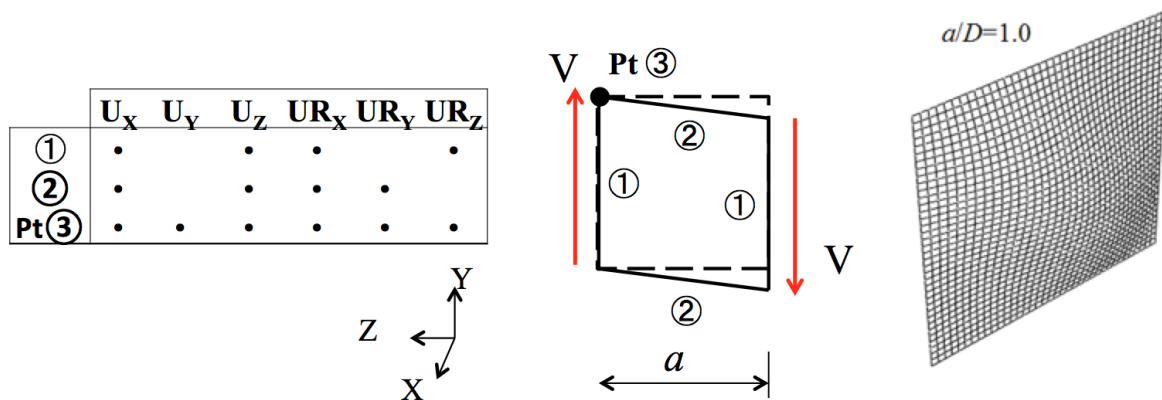


Figure 1: Boundary conditions of the FE model (left), and mesh density in first mode buckled shape (right). Location 3 is a point (Pt) on the upper left corner.

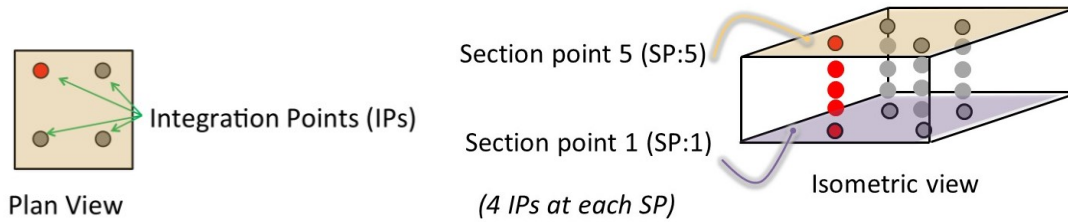


Figure 2: Integration points and section points on each shell finite element

126

127 To capture the plate transition from its initial unbuckled state to post-buckling behavior to

128 ultimate shear strength, nonlinear analyses were conducted using a modified Riks

129 procedure. These analyses require the insertion of an initial geometric imperfection to

130 perturb the mesh prior to loading, which allows the load-displacement curve to proceed

131 beyond the buckling bifurcation point and progress into the postbuckled behavior until V_u

132 is reached (Glassman et al., 2016). To create this initial geometric imperfection, the

133 eigenmode shape associated with the lowest elastic positive eigenvalue is multiplied by a

134 defined scale factor. Previous research by Garlock and Glassman (2014) found that a scale

135 factor of $D/10,000$ was sufficient for these models, and this scale factor was therefore

136 selected for the present study. Mesh convergence studies were conducted using an

137 eigenvalue extraction analysis. The final mesh selected is shown in Fig. 1, and equal to 37 x

138 37 elements (approximately 1.57 inches (40 mm) square each).

139

140 Using this approach, the FE solution for the elastic shear buckling load, V_{cr} , equaled 345

141 kips (1535 kN). This value has less than 1% error compared to a theoretical solution of

142 343 kips (1526 kN), which is obtained from Eq. (1):

$$\tau_{cr} = k \frac{\pi^2 E}{12(1-\nu^2) \left(\frac{D}{t_w} \right)^2} \quad (1)$$

Pre-Print Copy: Garlock et al. (2019). "Post-buckling mechanics of a square slender steel plate in pure shear." *Engineering Journal (AISC)*, Vol. 56, No. 1, pp. 27-46.

143 In Eq. (1), τ_{cr} is the elastic shear buckling stress, E is Young's modulus, ν is Poisson's ratio, D
144 is the depth of the plate, t_w is the plate thickness, and k is the elastic shear buckling
145 coefficient. The value of k is a function of the span-to-depth (aspect) ratio (a/D) of the plate
146 and the boundary conditions applied to its edges (Timoshenko and Gere, 1961). For a plate
147 with $a/D = 1$ and simply supported on all four edges, k equals 9.34. D/t_w is the slenderness
148 ratio, which is a measure of how susceptible the plate girder is to web shear buckling. The
149 elastic critical shear buckling load, V_{cr} , is calculated by multiplying Eq. (1) by $D \cdot t_w$.

150
151 The modeling approach described above has also been validated via comparison to
152 experimental test data for various a/D and D/t_w ratios. Glassman and Garlock (2016)
153 considered the results of 16 previous experiments whose results are published in Basler et
154 al., 1960; Bergfelt et al., 1968; Kamtekar et al., 1972; Rockey and Skalmoud, 1972; Evans et
155 al., 1977; Narayanan and Rockey, 1981. Glassman and Garlock's (2016) FE models used the
156 same setup conditions as discussed above and showed very close agreement with the
157 ultimate post-buckling shear capacity, V_u , of each plate. Specifically, the FE models
158 predicted V_u values to within $\sim 10\%$ of the published experimental values with one
159 exception where the flange-to-web thickness ratio (t_f/t_w) was quite large compared to
160 other tests (thus influencing that plate's boundary conditions more so than the other
161 validation cases).

162 **3. Results**

163 *3.1 Sign Conventions and Definitions*

164 To properly interpret the finite elements results, the definitions and sign conventions of the
165 stresses, moments, and rotations are defined in this paper as follows, in the context of the
166 Abaqus output:

- 167 • Tensile stresses are positive and compressive stresses are negative.
- 168 • SP:1 and SP:5 refer to the section points on the two surfaces of the plate as shown in
169 Fig. 2.
- 170 • The element stresses, σ_1 , σ_2 , and σ_{12} are defined in Fig. 3a in the positive direction.
- 171 • Maximum principal stresses (σ_{\max}) are the maximum positive value, thus typically
172 corresponding to maximum tensile stresses. If no tension is present, the value will be
173 negative, thus corresponding to the minimum compressive value (see Fig. 3b).
- 174 • Minimum principal stresses (σ_{\min}) are the maximum negative value, thus typically
175 corresponding to maximum compressive stresses. If no compression is present, the
176 value will be positive, thus corresponding to the minimum tensile value (see Fig. 3b).
- 177 • Von Mises stresses are defined for the principal plane stress condition defined by Eq.
178 (2), where σ_y is the yield stress. Fig. 4 plots this yield surface.

179
$$\sigma_y^2 = \sigma_{\max}^2 + \sigma_{\min}^2 - \sigma_{\max} \sigma_{\min} \quad (2)$$

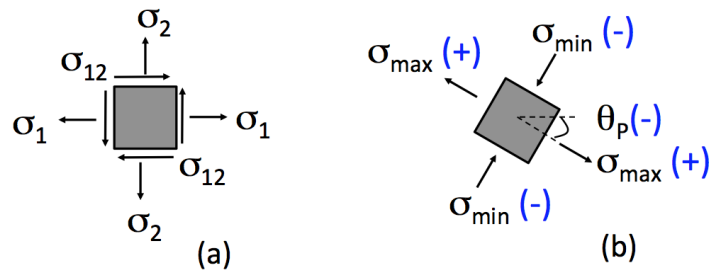


Figure 3: (a) Positive stresses on element; (b) Principal stresses and principal stress direction (with Abaqus sign convention in parenthesis).

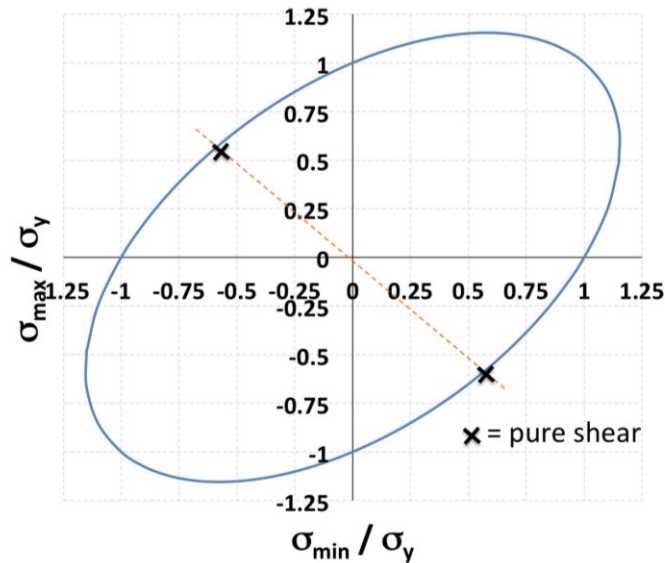


Figure 4: von Mises yield surface

180

181 Fig. 5 shows the shear force-deformation plot with V_{cr} and V_u for this plate labeled for
 182 clarity. Deformation is measured at the lower right corner of the plate as shown by the dot
 183 in the inset figure. Note that the plot can be divided into three phases of shear loading.
 184 Phase I represents the elastic state prior to buckling. In Phase II, the plate has exceeded V_{cr}
 185 but still exhibits nearly linear behavior. In Phase III, the plate's force-deformation behavior
 186 becomes highly nonlinear. For this plate, the boundary between Phases II and III lies
 187 approximately at the shear halfway between V_{cr} and V_u . In the following sections, the

188 stresses and strains throughout the plate will be evaluated at two values of loading: (1) in
189 Phase II at $V = 1.15 \cdot V_{cr}$ (when the plate has recently buckled), and (2) in Phase III at V_u
190 (when the plate has reached its peak shear load during post-buckling response).

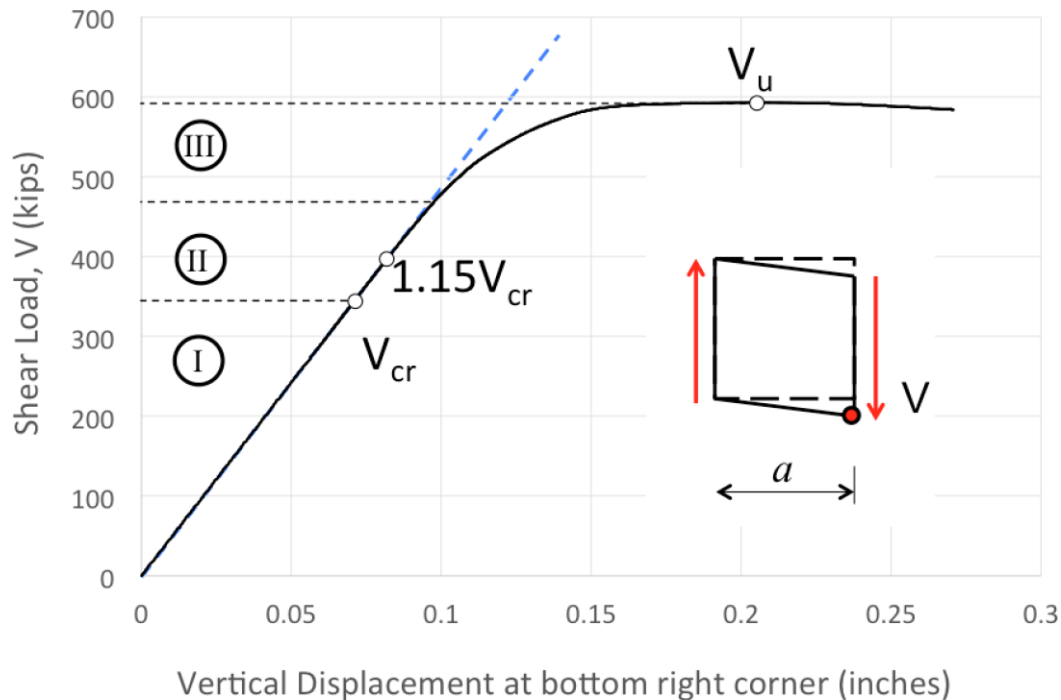


Figure 5. Shear displacement of the plate, with V_{cr} and V_u labeled.

191

192 3.2 Ultimate Shear Post-buckling Load, V_u , and Deformation

193 Fig. 6 illustrates the final deformed shape at the ultimate (post-buckling) shear load, V_u ,
194 which for this plate equals 593 kips (2636 kN). The out-of-plane deformations are
195 manifested in three half-wavelengths or bulges from Point B to Point D. The surface shown
196 in Fig. 6 represents the SP:5 face from Fig. 2. Therefore, along the 'tension field' (from
197 Point A to Point C, where the red color represents maximum out-of-plane positive
198 displacement), it will be shown that the SP:5 stresses will be in tension and SP:1 stresses
199 will be in compression due to the significant bending in the plate. Conversely, in Fig. 6

Pre-Print Copy: Garlock et al. (2019). "Post-buckling mechanics of a square slender steel plate in pure shear." *Engineering Journal (AISC)*, Vol. 56, No. 1, pp. 27-46.

200 where the dark blue color shows large negative displacement, SP:5 stresses will be in
201 compression and SP:1 stresses will be in tension. A thorough analysis of the stresses will
202 be discussed in sections to follow, where it will be shown that the plate bending due to this
203 post-buckling out-of-plane deformation dominates the response when V_u is reached.

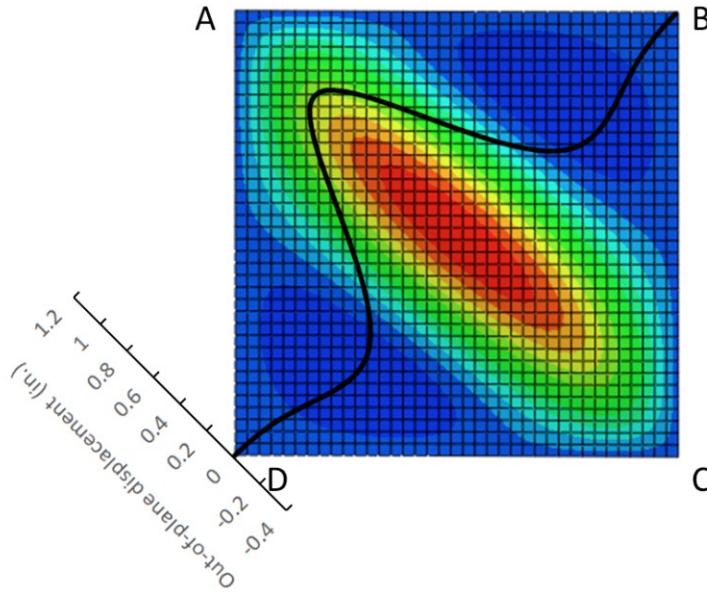


Figure 6: Deformed shape contour at V_u , with out of plane deformation plot superimposed (dark black line). The face shown (front face) corresponds to SP:5; the back face (not shown) corresponds to SP:1 (see Fig. 2).

204

205 3.3 Plate Behavior Just After Elastic Buckling

206 Before the plate reached the elastic shear buckling load V_{cr} , the FE results were consistent
207 with the theoretical behavior of a plate under pure shear: the angle of the principal stress,
208 θ_p , was 45° and the principal stresses in tension and compression (σ_{max} and σ_{min} ,
209 respectively) were equal and opposite to one another and also equal to the shear stress
210 ($V/(D \cdot t_w)$, where V is the applied load). Note that Abaqus does not output θ_p - this value
211 was derived using σ_1 , σ_2 , and σ_{12} with the well-established equation based on Mohr's circle.
212 In this section, the state of the plate when the shear $V = 1.15 \cdot V_{cr}$ (i.e. near the beginning of

213 post-buckling behavior) is examined to enable a comparison to ultimate post-buckling
214 behavior when V_u is reached. The following behavior is observed:

- 215 • *Principal Stress Direction, θ_p* : Fig. 7 plots the θ_p contours for $V/V_{cr} = 1.15$. It can be seen
216 that this angle has not changed significantly from the pre-buckling state when this angle
217 was 45 degrees.
- 218 • *Principal Stresses*: Fig. 8 plots the σ_{min} and σ_{max} contours for $V/V_{cr} = 1.15$. None of these
219 stresses have reached yield (50 ksi, 345 MPa), and the magnitude of σ_{min} (compressive
220 principal stress) is comparable to that of σ_{max} (tension principal stress). At an elastic
221 buckling load of 344 kips (1532 KN), the elastic buckling stress theoretically equals
222 13.7 ksi (95 MPa). At $V = 1.15 \cdot V_{cr}$, Fig. 8 shows that both σ_{min} and σ_{max} have generally
223 increased beyond 13.7 ksi.
- 224 • *von Mises Stresses*: Fig. 9 plots the von Mises stress contours for $V/V_u = 1.15$. As would
225 be expected, the stresses are shown to be well below yield (50 ksi).

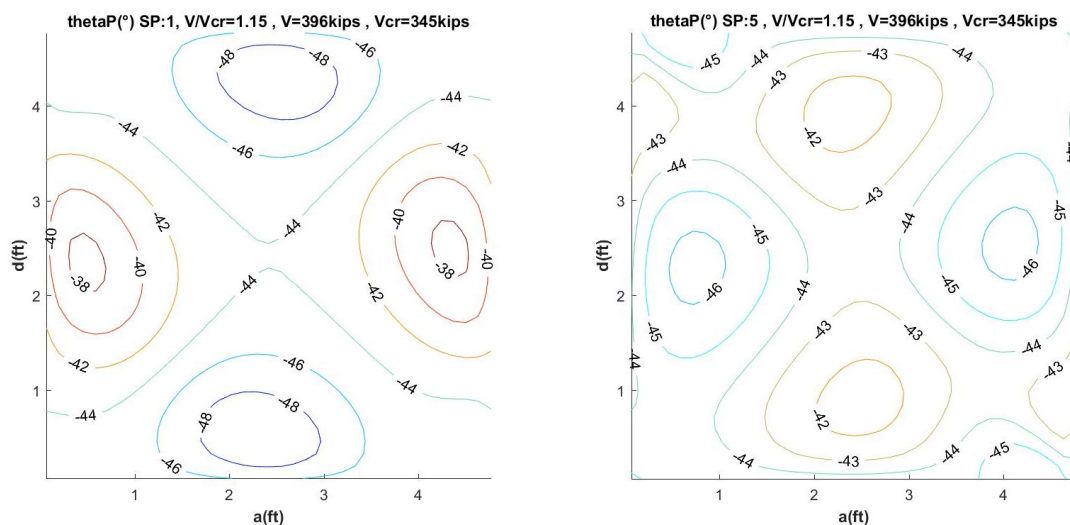


Figure 7: Principal stress direction, θ_p , for $V/V_{cr} = 1.15$ in degrees. Left = SP:1, Right = SP:5 (See Figs. 2, 3).

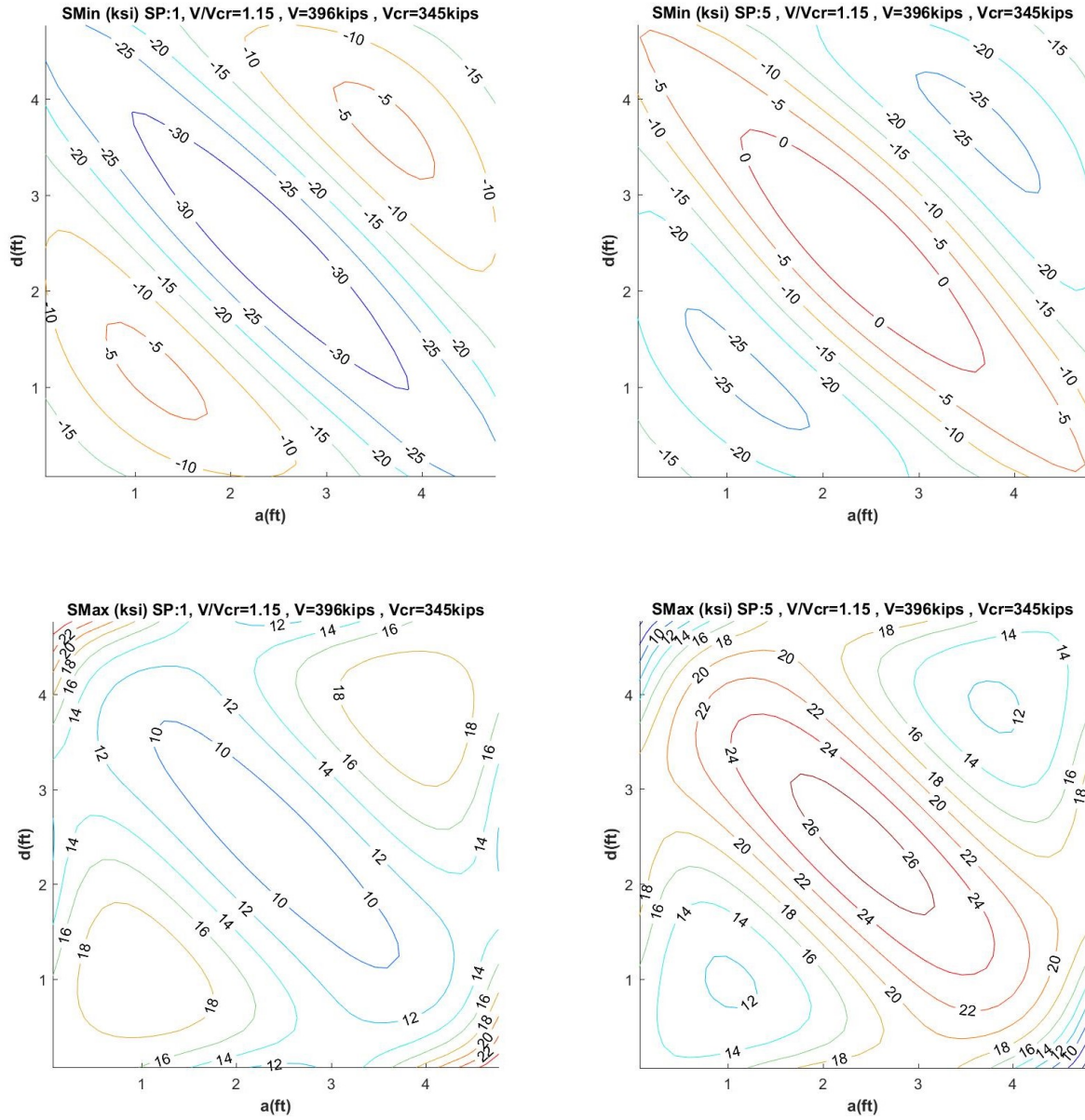


Figure 8: Principal stresses σ_{min} (top) and σ_{max} (bottom) for $V/V_{cr} = 1.15$ (ksi). Left = SP:1, Right = SP:5 (See Figs. 2, 3)

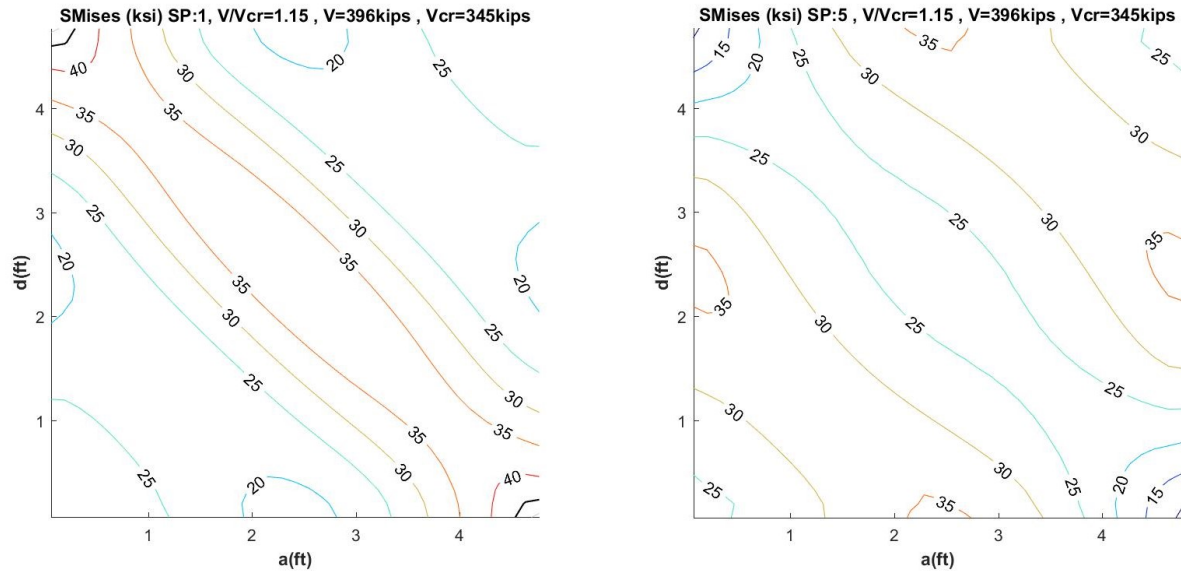


Figure 9: von Mises Stresses for $V/V_{cr} = 1.15$ (ksi). Left = SP:1, Right = SP:5 (See Figs. 2, 3, 4).

226

227 Though the contour patterns are similar, Figs. 7 through 9 all show some variation in the
228 magnitudes of plotted results between the SP:1 and SP:5 faces of the plate. More significant
229 levels of variation are shown for the principal and von Mises stresses in Figs. 8 and 9. The
230 stress patterns on the opposing SP:1 and SP:5 faces highlight the emergence of bending
231 moment through the thickness of the postbuckled plate in addition to in-plane stress.

232 These moments are caused by second-order bending due to in-plane compression of the
233 buckled plate. Each of the three half-wavelengths of this prototype's buckled shape
234 experiences "bulging" as the top right and bottom left corners of the plate (from B to D in
235 Fig. 6) are pushed closer together by the pure shear force.

236

237 3.4 Plate Behavior at the Ultimate Shear Post-buckling Load, V_u

238 The following observations are made regarding the stress state of the plate when the shear,
239 V , equals the ultimate shear post-buckling load, $V_u = 593$ kips (2636 kN).

- 240 • *Principal Stress Direction, θ_p* : Fig. 10 plots the θ_p contours for $V = V_u$. It can be seen that
 241 this angle is no longer ~ 45 degrees and now varies between 15 and -65 degrees. Also,
 242 the values are now significantly different on each face (SP:1 and SP:5) since the
 243 principal stresses are also different on each face. θ_p is shown to be largely dependent
 244 on the out-of-plane postbuckled deformation.

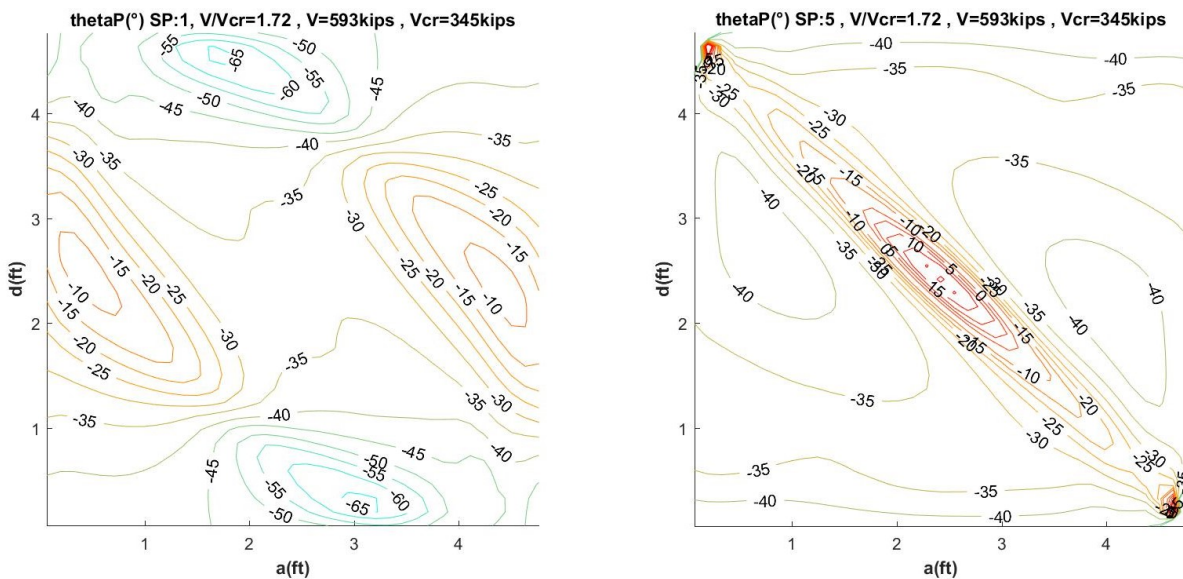


Figure 10: Principal stress direction, θ_p , for $V = V_u$ in degrees. Left = SP:1, Right = SP:5 (See Figs. 2, 3).

- 245 • *Principal Stresses*: Fig. 11 plots the σ_{min} and σ_{max} contours for $V = V_u$. Both σ_{min} and σ_{max}
 246 have reached yield in the regions marked by the bold lines encircling grey shading. The
 247 magnitudes, signs (positive, negative), and locations of these stresses are related to the
 248 out-of-plane postbuckled deformation (and bending) of the plate at V_u as seen
 249 previously in Fig. 6. The σ_{max} contours for SP:5 in Fig. 11 show a distinct band of
 250 yielding in the tension field direction, which generally supports the assumptions in the
 251 current state of practice. However, the σ_{max} contours for SP:1 show much lower
 252 maximum stress (actually remaining negative in compression) in this same region due
 253 to bending. The σ_{min} stresses at yield are located along the tension field for SP:1 and

254 along two smaller bands that are parallel to the tension field at SP:5. These stresses
255 represent the compression face of bending in the buckled half-wavelength bulges along
256 the diagonal. The emergence of these large compressive stresses on the SP:1 face
257 indicates that the large tensile stresses in the tension field on the SP:5 face are caused
258 by a combination of in-plane stress and second-order bending.

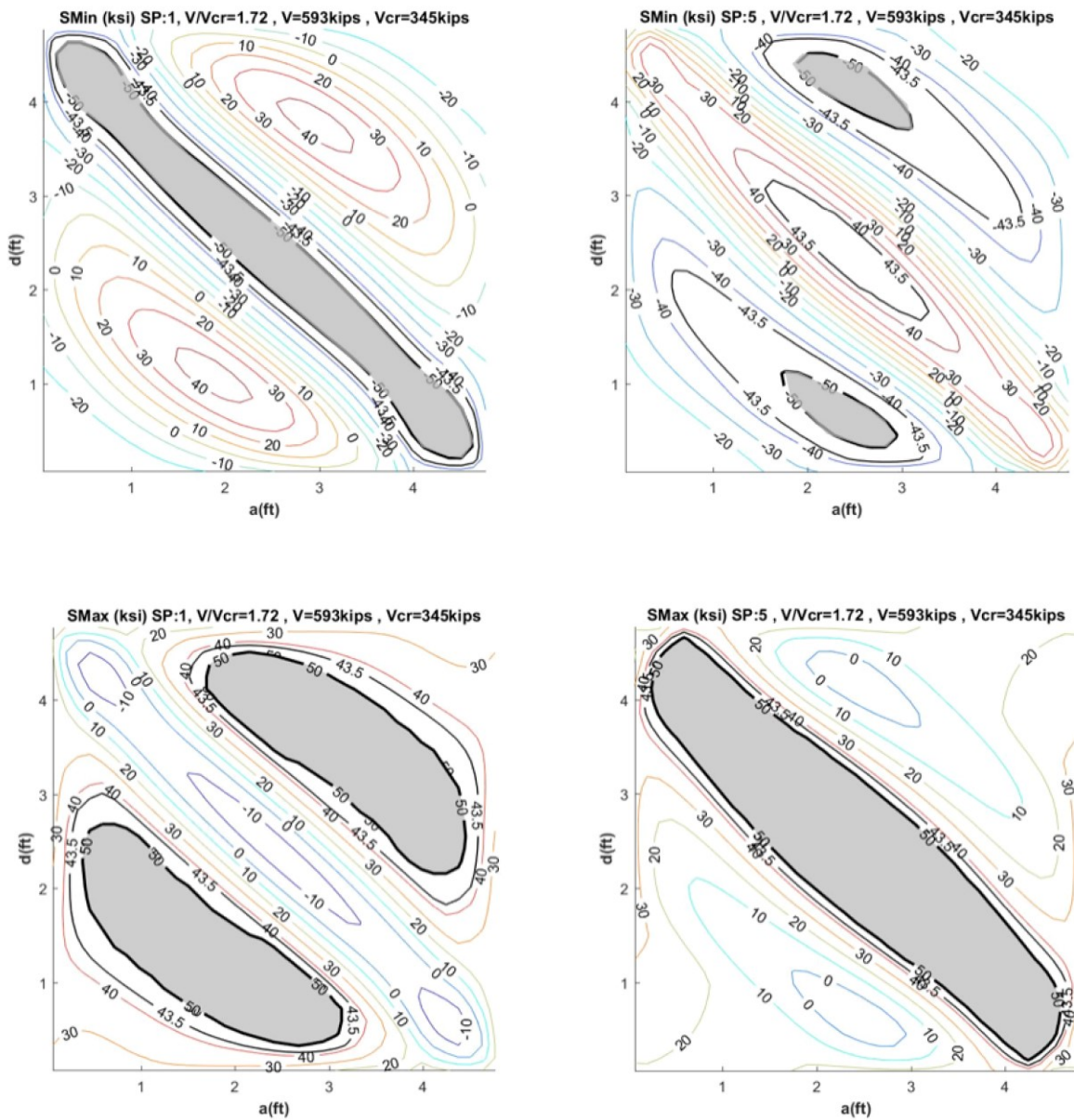


Figure 11: Principal stresses σ_{min} (top) and σ_{max} (bottom) for $V = V_u$ (ksi). Left = SP:1, Right = SP:5 (See Figs. 2, 3). Grey shaded regions represent areas that have reached yield.

259

260 • *von Mises Stresses*: Fig. 12 plots the von Mises stress contours for $V = V_u$. Nearly the
261 entire plate surface has reached the von Mises yield condition (at 50 ksi, again shown
262 with bold lines and grey shading) on both faces. At ultimate shear, the plate
263 experiences a near saturation of von Mises yielding due to the combination of internal
264 forces that develops in its buckled shape. Fig. 12 shows that face SP:5 experiences a
265 more widespread saturation of von Mises yielding than SP:1, which has a distinct band
266 of yielding along the tension field diagonal and two other 'pockets' of yield parallel to it.
267 Note that bending-induced compression stress has caused von Mises yielding in the
268 tension field diagonal on face SP:1 rather than in-plane tensile stresses. This deviates
269 from the current state of practice, which assumes in-plane stress to be the primary
270 contributor to reaching ultimate shear capacity.

271 • *Equivalent Plastic Strains*: Fig. 13 plots (for $V = V_u$) the equivalent plastic strains
272 normalized by the yield strain ($\epsilon_y = 0.001725$) to provide a relative measurement of
273 ductility utilization. This value quantifies the plastic strain as related to von Mises
274 plasticity. Comparing to Figure 12, one sees that these strain values are greater than
275 zero only where yield has been reached. In the tension field region, the equivalent
276 plastic strains are larger than 2 times ϵ_y on one face and just slightly greater than ϵ_y on
277 the other face. The material model assumes strain hardening begins at a strain value
278 equal to 0.02. From Fig. 12, one can infer that the strains in the plates are well below
279 this value.

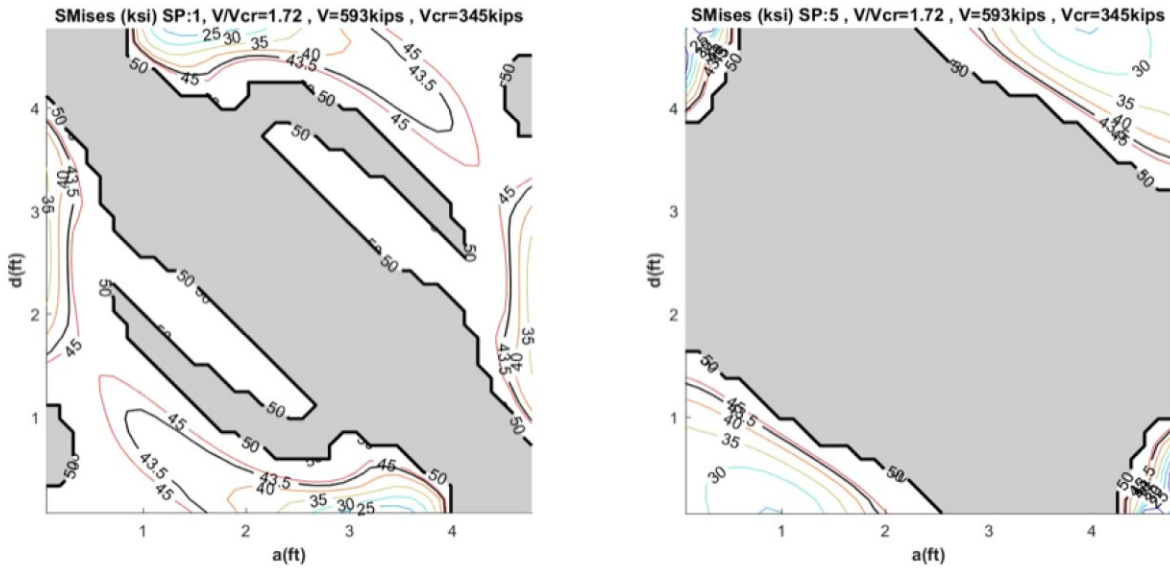


Figure 12: von Mises Stresses for $V = V_u$ (ksi). Left = SP:1, Right = SP:5 (See Figs. 2, 4). Grey shaded regions represent areas that have reached yield.

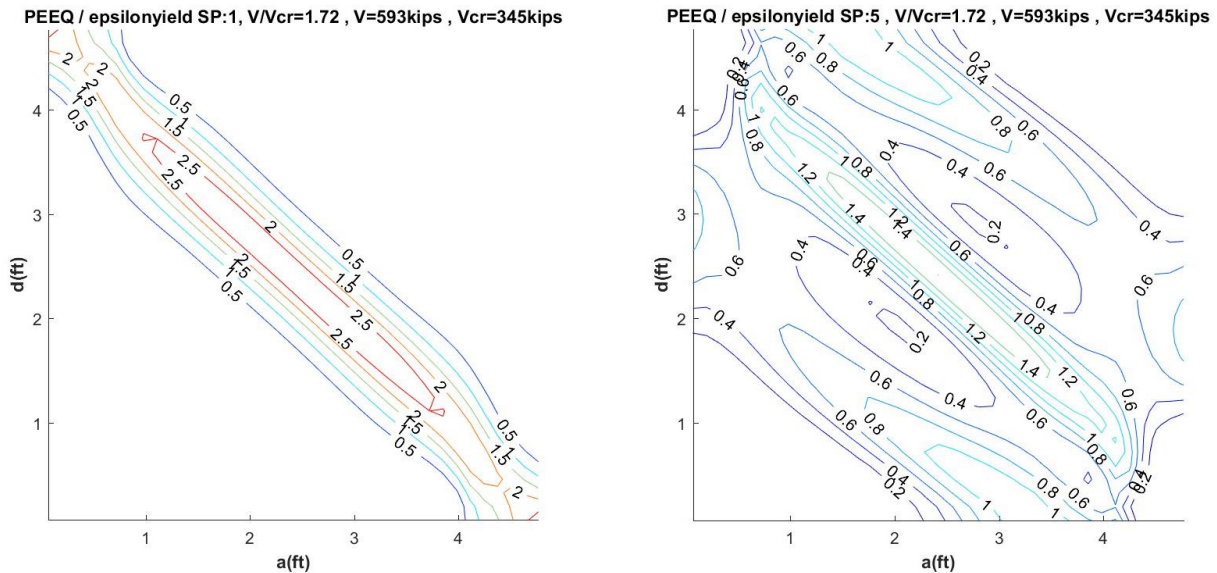


Figure 13: Equivalent plastic strains normalized by yield strain ($\epsilon_y = 0.001725$) for $V = V_u$. Left = SP:1, Right = SP:5.

280

281 *3.4 Bending Stresses at the Ultimate Shear Post-buckling Load, V_u*

282 The results presented thus far indicate that bending through the thickness of the plate due

283 to postbuckled out-of-plane deformations has a large effect on the stress distribution. In

284 this section, the axial stress is distinguished from the bending stress for both σ_1 and σ_2 (see

285 Fig. 3). The stresses are output at the 5 section points (SPs, i.e. the through-thickness
286 integration points) through the shell element thickness (see Fig. 2). Abaqus outputs the
287 total stress and the average section stress (i.e., membrane axial stress) at each SP. The
288 bending stress is calculated by subtracting the membrane stress from the total stress.

289

290 Fig. 14 presents the axial (in-plane) and bending (second-order) stresses through the plate
291 thickness for $V = V_u$ (ksi). The left plot represents stress patterns typically seen along the
292 tension field. These stresses are nearly linear through the depth and become slightly
293 nonlinear as it approaches the top and bottom surface, where the stresses, considering von
294 Mises plasticity, have reached yield. The right plot represents stress patterns typically seen
295 outside of the tension field (near upper right and lower left corners). In these regions the
296 stresses are linear through the depth and smaller than those in the tension field.

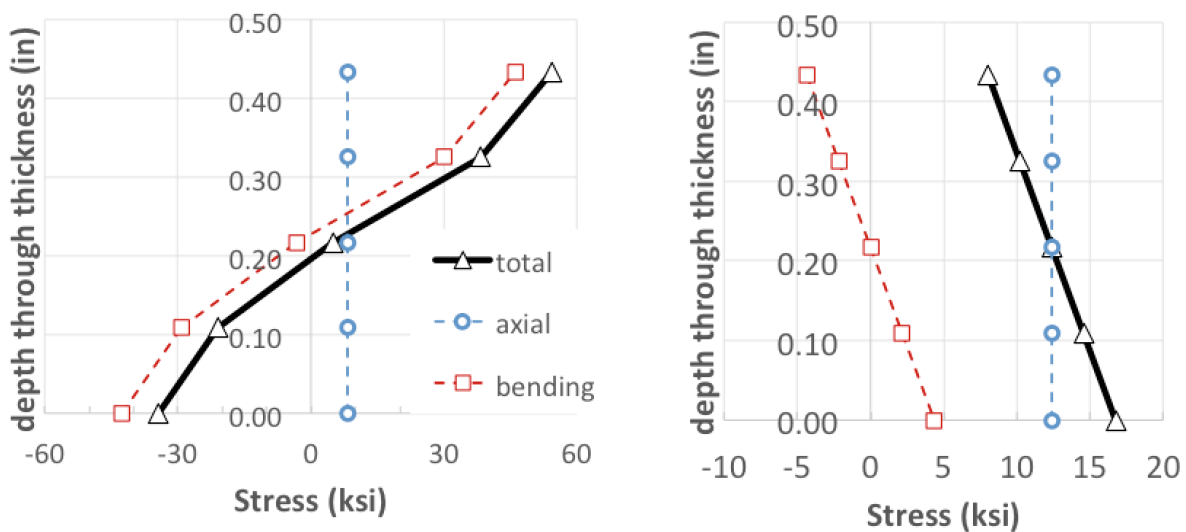
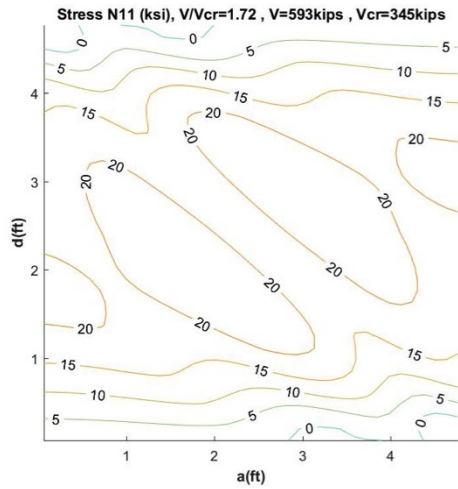


Figure 14: Plot of axial and bending stresses in the σ_1 direction through the plate thickness for $V = V_u$. Left = representative stresses along tension field; Right = representative stresses outside of tension field (near upper right and lower left corners).

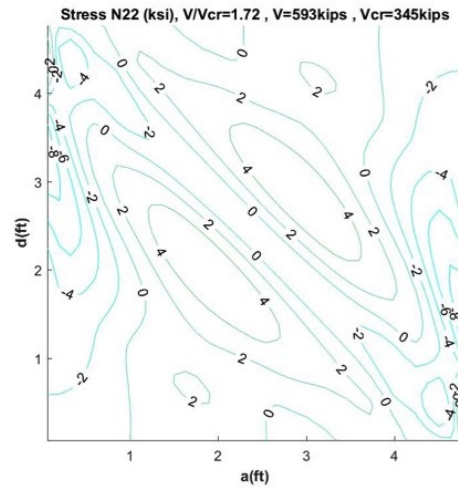
297

Pre-Print Copy: Garlock et al. (2019). "Post-buckling mechanics of a square slender steel plate in pure shear." *Engineering Journal (AISC)*, Vol. 56, No. 1, pp. 27-46.

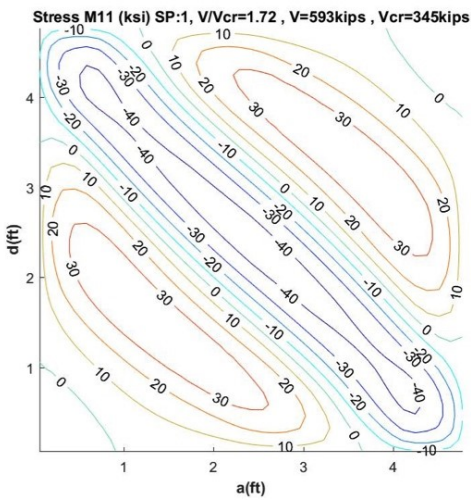
298 Fig. 15 presents the axial stress (top row) and bending stress at SP:1 and SP:5 (middle and
299 lower rows) for both σ_1 (left column) and σ_2 (right column). It is clearly seen that bending
300 stresses dominate since their magnitudes are nearly 2 times larger than axial stress for σ_1
301 and on the order of 10 times larger for σ_2 . These plots clearly show that second-order
302 moment in the postbuckled shape makes a significant contribution to the onset of ultimate
303 shear capacity.



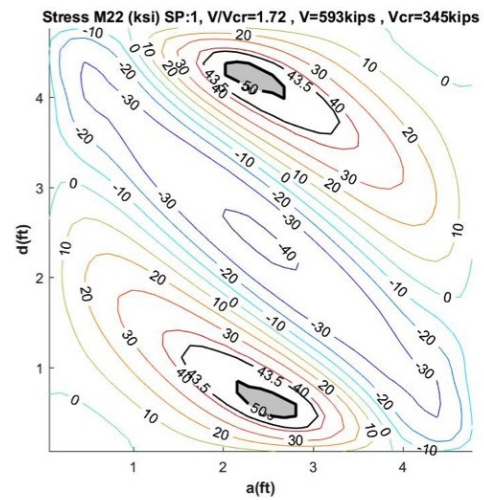
(a1) axial stress – for σ_1 direction



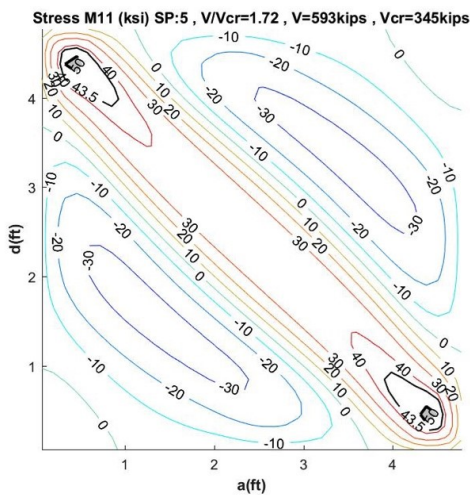
(a2) axial stress – for σ_2 direction



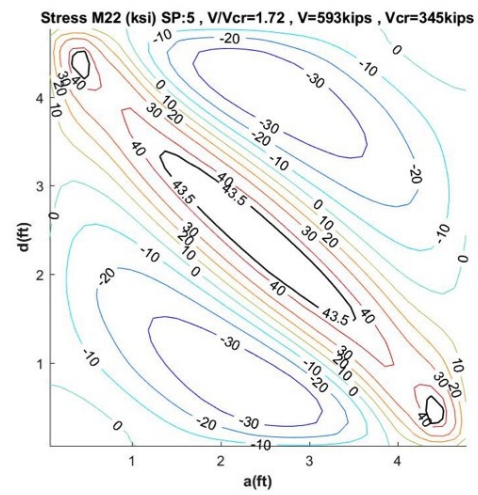
(b1) bending stress – for σ_1 direction; SP:1 face



(b2) bending stress – for σ_2 direction; SP:1 face



(c1) bending stress – for σ_1 direction; SP:5 face



(c2) bending stress – for σ_2 direction; SP:5 face

Figure 15: Axial and bending stresses for $V = V_u$ (ksi). Left figures are for σ_1 and right are for σ_2 .

304 Fig. 16 provides additional illustration of the bending in the plate by plotting σ_{\min} and σ_{\max}
305 at the shell element in the center of the plate against the vertical plate displacement at the
306 bottom corner for both SP:1 and SP:5. The point of elastic shear buckling when V_{cr} is
307 reached is clearly shown where SP:1 and SP:5 bifurcate for both σ_{\min} and σ_{\max} . This
308 increasing divergence clearly indicates the onset of second-order bending moment through
309 the thickness of the plate. At V_u , SP:1 and SP:5 are significantly different for both σ_{\min} and
310 σ_{\max} .

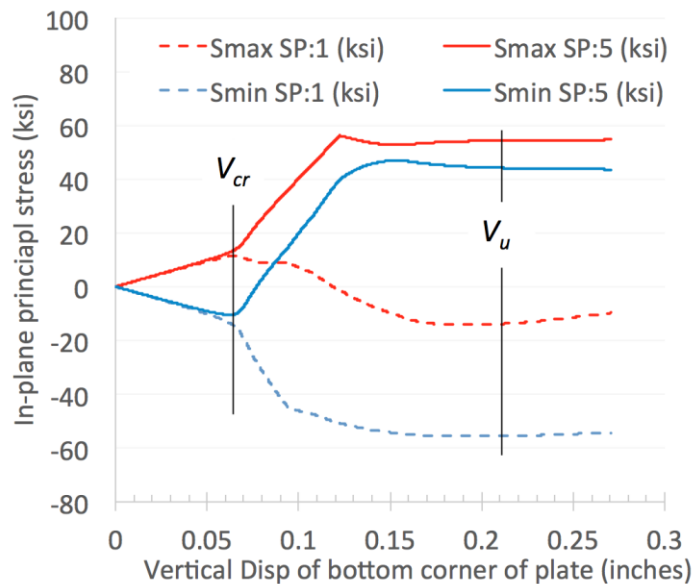


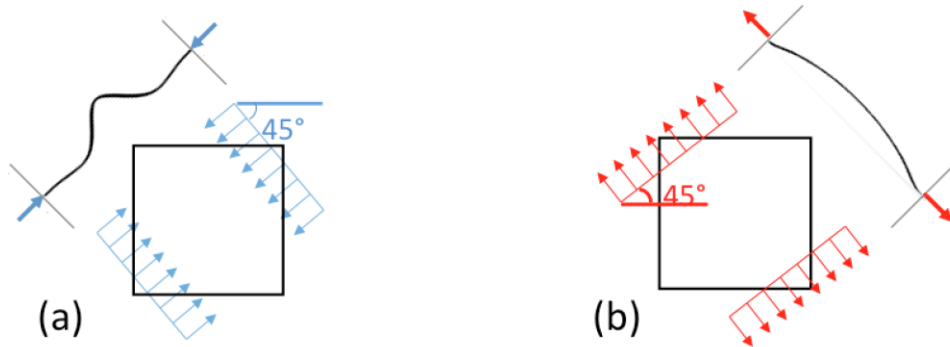
Figure 16: σ_{\min} (Smin) and σ_{\max} (Smax) for the shell element in the center of the plate on both surfaces SP:1 and SP:5. Elastic shear buckling, V_{cr} , and ultimate shear post-buckling, V_u , are labeled.

311
312 *3.5 Membrane Stresses at the Ultimate Shear Post-buckling Load, V_u*
313 It is worthwhile to observe the influence of stresses independent of bending effects. Thus,
314 this section discusses the membrane stresses (i.e., the axial stresses), which are equal to
315 the membrane forces divided by the plate thickness. Fig. 17 plots the membrane stresses
316 along the diagonal directions of the compression and tension paths (at negative 45 degrees
317 and positive 45 degrees, respectively) when the shear load equals V_u . Fig. 17(a) marks with

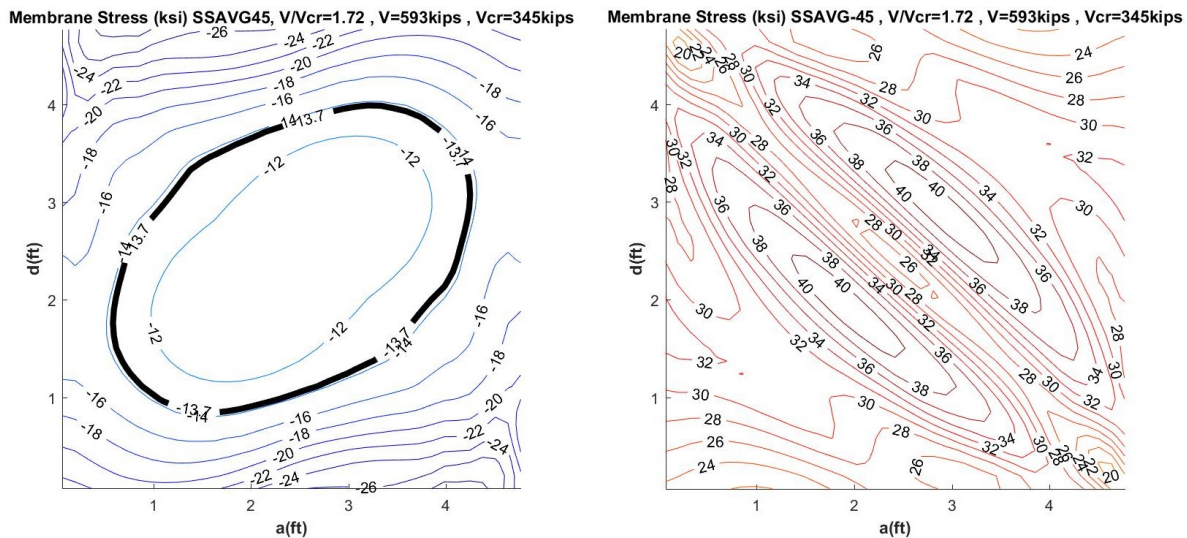
Pre-Print Copy: Garlock et al. (2019). "Post-buckling mechanics of a square slender steel plate in pure shear." *Engineering Journal (AISC)*, Vol. 56, No. 1, pp. 27-46.

318 a thick bold line the 13.7 ksi (95 MPa) contour, which represents the stress at the elastic
319 shear buckling load, V_{cr} . Inside the dark bold line, stresses are at or below 13.7 ksi, while
320 outside of this region compressive stresses reach up to 26 ksi. This figure illustrates that
321 compression continues to grow beyond V_{cr} , which is contrary to tension field theory
322 assumption. Yoo & Lee (2006) have similarly shown that compression stresses will
323 increase beyond elastic buckling, predominantly along the edges of the web panel. Fig.
324 17(b) shows that tension stresses range from 24 to 40 ksi – the tension field has a stiffer
325 load path as illustrated in Fig. 17's conceptual sketches, which translates into larger
326 stresses.

327



328



329

330 Figure 17: (a) Compressive and (b) tensile membrane stresses (ksi) at V_u acting along the 45-
 331 degree diagonal directions shown.

332

333 Fig. 18 plots the diagonal membrane stresses vs. shear load for every element along the
 334 corner-to-corner diagonal of the tension path (Fig. 18(a)) and compression path (Fig.
 335 18(b)). One curve is plotted for each element, and since the results are perfectly
 336 symmetrical, it appears as though only half the elements on each diagonal are plotted. The
 337 orange curves represent the elements that are inside of the bold black contour of Fig. 17(a),
 338 i.e. with compressive stresses equal to or less than 13.7 ksi at V_u . Green lines represent the
 339 elements that fall outside of this region. Fig. 18(a) shows that all of the elements in the
 340 tension diagonal continue to increase beyond the 13.7 ksi reached at V_{cr} .

341

342 Fig. 18(b) shows that after elastic buckling, compressive stresses continue to increase for
343 all elements along the compression diagonal. An overall reduction in the rate of stress
344 increase is observed after elastic buckling, with elements inside of the 13.7 ksi ring
345 experiencing a larger reduction than elements outside of the ring. While Fig. 17(a) shows
346 that at V_u some compressive stresses are below 13.7 ksi (σ_{\min} at V_{cr}), Fig. 18(b) shows that
347 these elements reached stresses larger than 13.7 ksi before decreasing prior to failure.

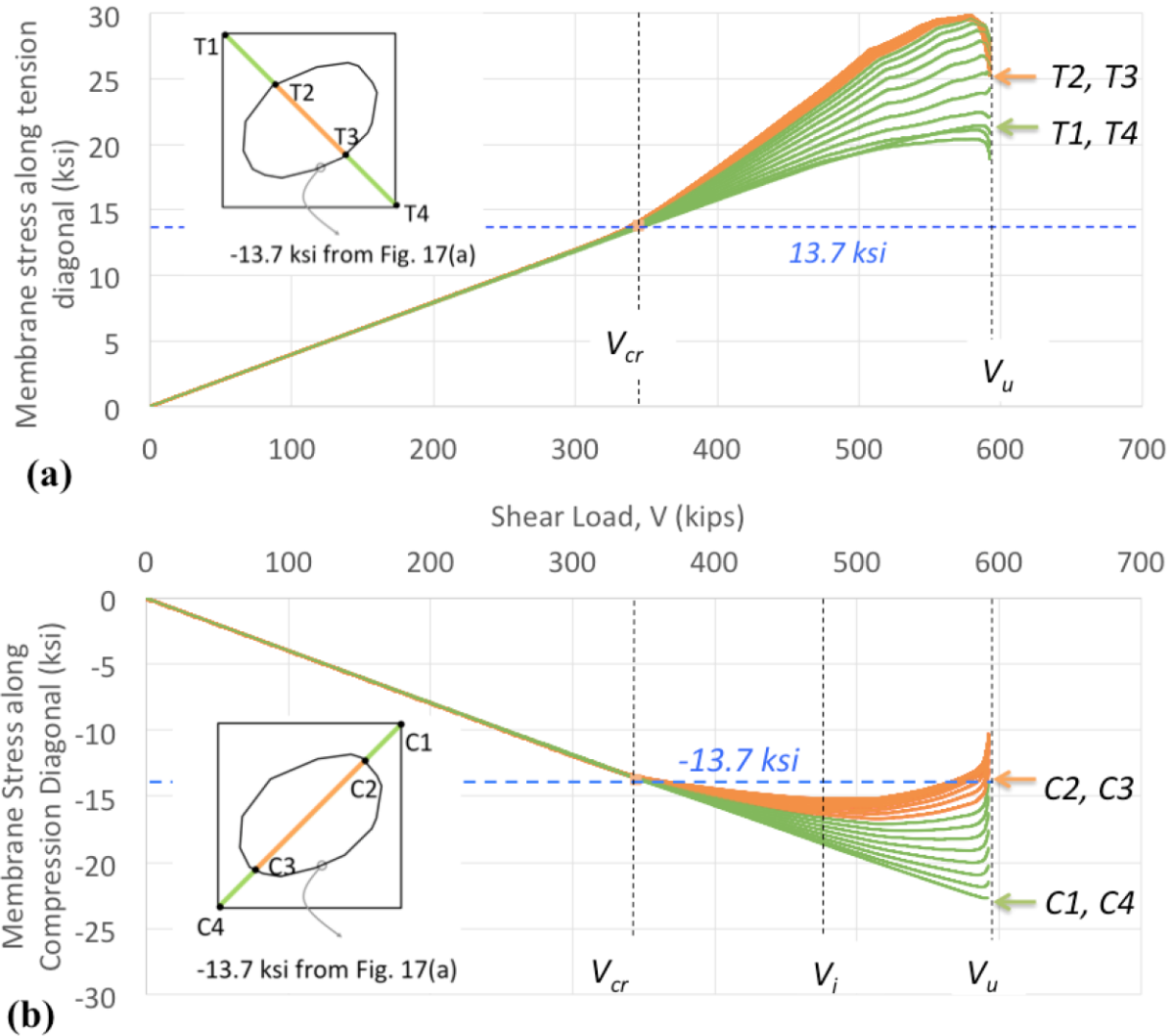
348

349 The "intermediate" shear load V_i marked in Fig. 18(b) represents the point at which an
350 element along the compression diagonal first experiences a stress decrease. Note how V_i
351 correlates to the transition from Phase II to Phase III in Figure 5. A change in stiffness in
352 the load-deformation behavior occurs when the compression diagonal elements near the
353 center of the plate experience reduced membrane stresses. The additional load carrying
354 capacity of a plate beyond V_{cr} is equal to V_u minus V_{cr} (see Fig. 5). Figs. 5 and 18 together
355 show that about half of that additional capacity occurs while the compression load path is
356 still in place and compressive stresses are increasing throughout. Compression is thus
357 playing a clear role in developing the post-buckling shear strength.

358

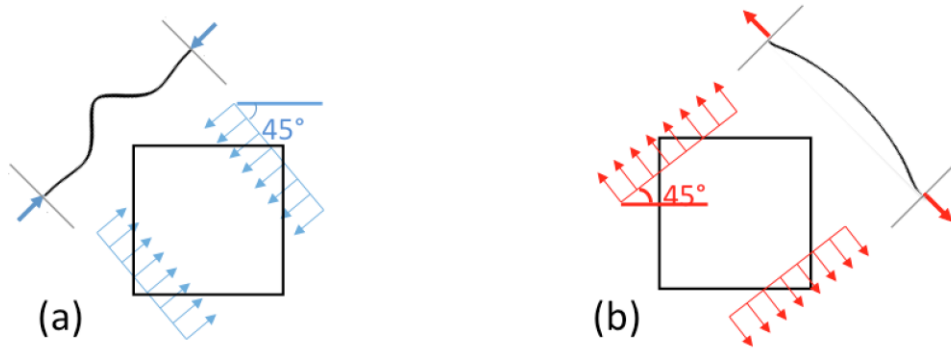
359 The membrane stresses along the diagonal directions of the compression and tension paths
360 (at negative 45 degrees and positive 45 degrees, respectively) at V_i are shown in Fig. 19. It
361 is observed that the compressive stresses in all elements do indeed exceed that at V_{cr} (13.7
362 ksi). In the center of the plate, the tensile membrane stresses are larger than the

363 compressive membrane stresses (24 ksi vs 15.5 ksi, respectively), but at the edges of the
364 web panel they are similar.

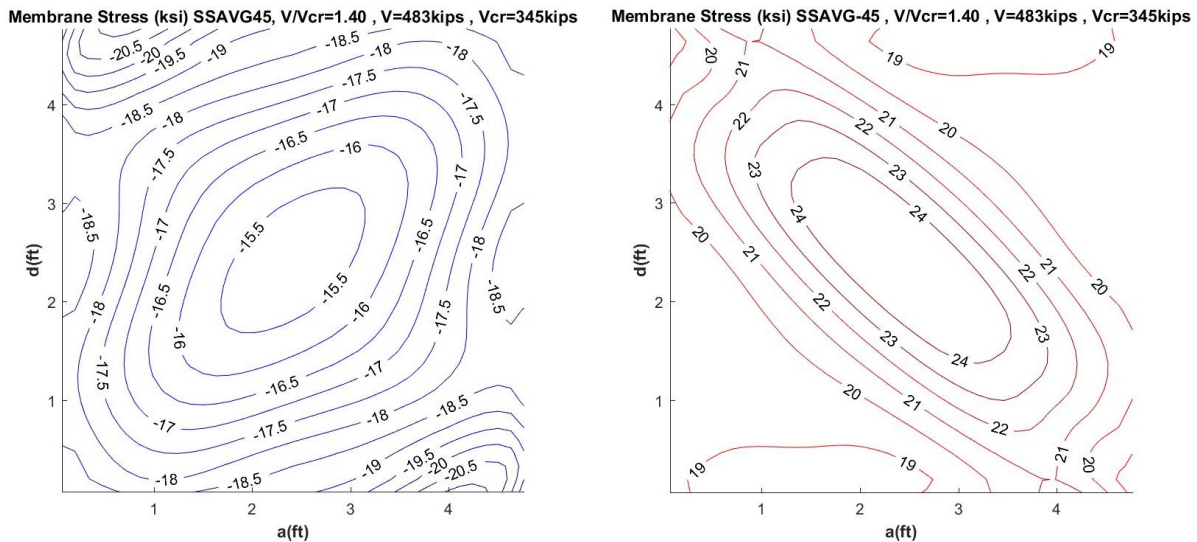


365
366 Figure 18: Plot of membrane stresses versus applied shear load for finite elements
367 along the (a) tension diagonal and (b) compression diagonal.

368



369



370




371 Figure 19: (a) Compressive and (b) tensile membrane stresses (ksi) at the intermediate
 372 shear load V_i (see Fig. 18(b)) acting along the 45-degree diagonal directions shown.
 373

374 **4. Interrupting the Compression Path**

375 The results presented in Section 3 indicate that compression and second-order bending
 376 stresses (due to large out-of-plane deformations) play an important role in the post-
 377 buckling performance of this slender plate. While it is not clear yet how the compression
 378 behavior directly contributes to V_u , studies that interrupt the compression field, as
 379 presented in this section, can provide some clues. To this end, the plate was modified in
 380 two ways: (1) by cutting the compression field corners by 16% of the depth D (model name
 381 = CUT), thus reducing the area by 3%; and (2) by cutting slits near the corners along the

382 compression field (model name = SLITS), thus reducing the area by 1%. Images of these
 383 models and the resulting V_{cr} and V_u values obtained from finite element analysis are shown
 384 in Table 1. Contour plots of the von Mises stress when the plate reaches V_u are shown for
 385 each case in Fig. 20. Contour plots of the equivalent plastic strains at V_u are shown for each
 386 case in Fig. 21.

Table 1: Finite element results of modified plates.

		V_{cr} (kips)	V_u (kips)
		(ratio to baseline)	
FULL (baseline)		344 (1.00)	593 (1.00)
CUT		428 (1.24)	594 (1.00)
SLITS		380 (1.10)	564 (0.95)

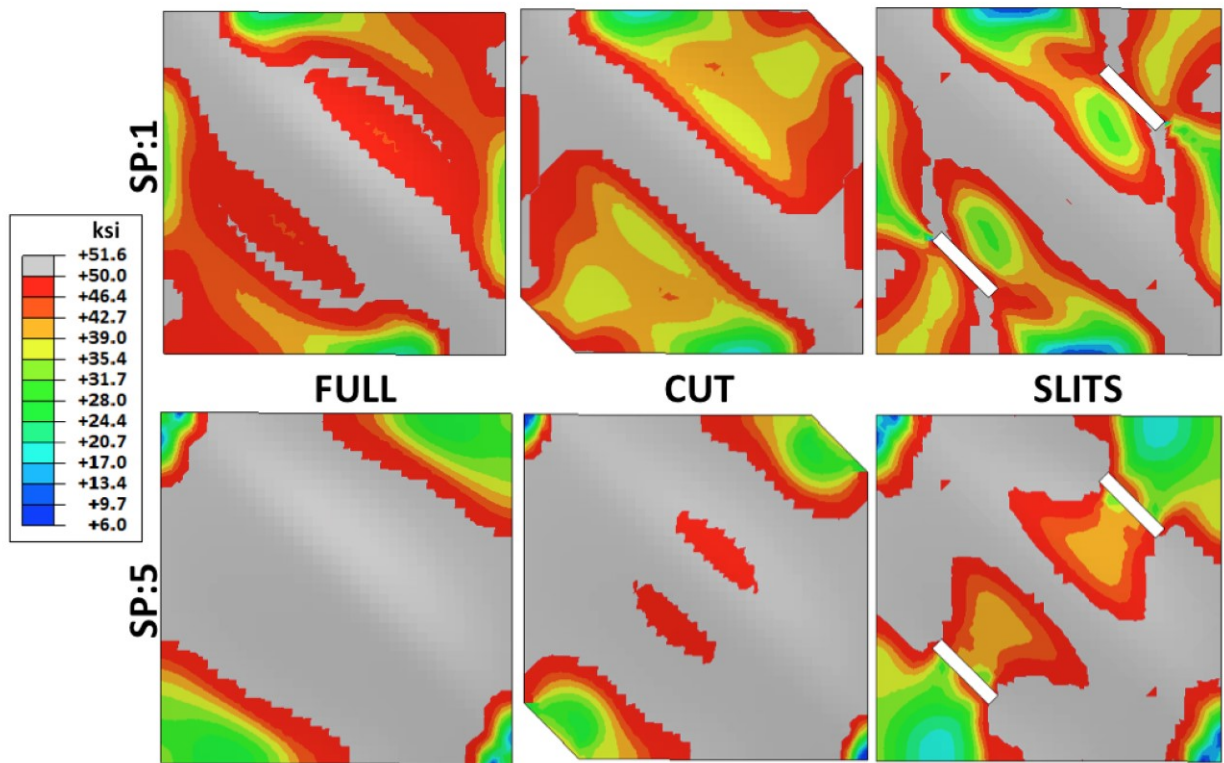


Figure 20: von Mises stresses at $V=V_u$ for the FULL plate, the CUT plate, and the plate with SLITS (units = ksi).

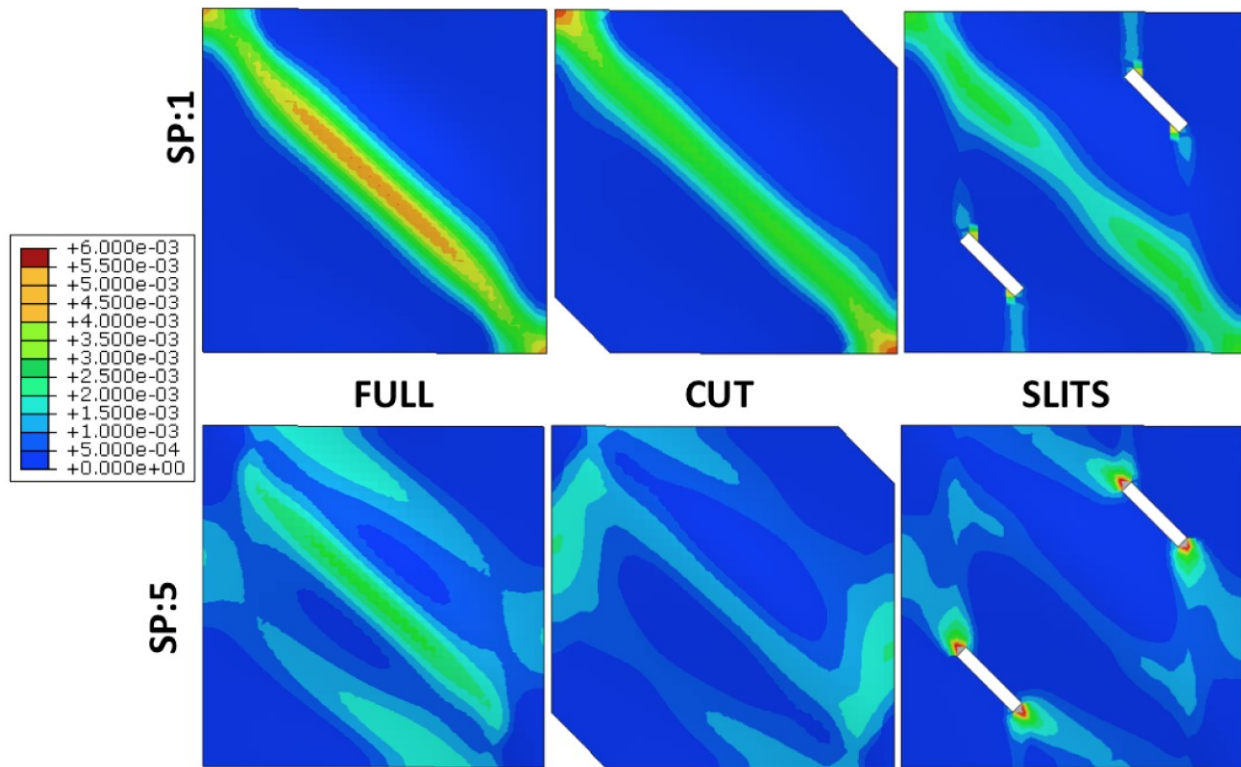


Figure 21: Equivalent plastic strains at $V = V_u$ for the FULL plate, the CUT plate, and the plate with SLITS

387

388 Table 1 shows that interrupting the compression field delays the onset of elastic buckling
389 and increases V_{cr} up to 24%. For the CUT case, V_u is unaffected since the cut corners do not
390 deter the development of von Mises stress patterns similar to the FULL original plate, as
391 shown in Fig. 20. For the SLITS case, the slits alter the von Mises stress patterns on the top
392 face of the plate (by interrupting the edges of the von Mises stress saturation), thus
393 reducing the ultimate shear capacity below the full plate model (a 5% reduction).

394

395 The plots of equivalent plastic strains in Fig. 21 show similar patterns to the von Mises
396 stress patterns. On the SP:1 face, these strains exceed zero only in the tension field, and all
397 three plates show similar strain patterns despite their modifications. Furthermore, the

398 magnitude of strain values is similar for all three plates. Although not shown, bending
399 stresses again dominate over membrane axial stresses for the CUT and SLITS cases as
400 discussed previously for the FULL case (described in detail via Fig. 15).

401

402 These results suggest that the elastic buckling load could be strategically modified to meet
403 a given design objective with relatively minor modifications to the plate. The ultimate
404 shear post-buckling load, however, is not significantly affected by these modifications.
405 Based on these results, the authors are now exploring new potential models of ultimate
406 plate post-buckling mechanics for thin plates which incorporate second-order bending of
407 the postbuckled shape. Also, the mechanical impact and construction/life-cycle
408 implications of the plate modifications will be examined in future research by the authors.

409

410 **5. Summary and Conclusions**

411 Post-buckling behavior of slender webs in steel plate girders has been a mainstay of plate
412 girder design for several decades on the basis of semi-empirical equations that were
413 originally developed in the 1960s. Though the existing state of practice is generally
414 conservative, the assumption of pure in-plane stress in response to shear loads after the
415 web has buckled does not capture the full mechanical responses of the thin plate. New
416 research by the authors has begun to reexamine the post-buckling behavior of thin steel
417 plates by considering the combined effects of in-plane stress and out-of-plane (second-
418 order) bending. This study utilized a previously validated finite element modeling
419 approach in Abaqus to analyze a prototype simply supported plate with an aspect ratio
420 equal to 1.0. The results of these analyses showed that out-of-plane bulging of the

421 postbuckled plate produces second-order bending moments due to compression along the
422 diagonal opposite the tension field.

423

424 Although the conclusions summarized below are based only on the plate dimensions of this
425 initial study, these results point to future research that is needed. The results are also
426 relevant to plates of other proportions that demonstrate shear post-buckling behavior that
427 is physically characterized by significant bulging/wrinkling on the diagonal (thus
428 generating potentially significant bending stresses through the thickness).

429 • At the ultimate shear post-buckling load, V_u , the angle of principal stress direction is no
430 longer 45 degrees and instead varies between 15 degrees (counter clockwise) and 65
431 degrees (clockwise).

432 • The stress distribution through the plate thickness was separated into pure planar (i.e.
433 axial) and bending (second-order) stresses. Bending stresses were found to be
434 significantly higher than the pure planar stresses at the ultimate post-buckling shear
435 load. These stresses are created by second-order compression of the plate's buckled
436 shape (i.e., the buckled half-wavelengths that bulge out-of-plane along the length of the
437 compression field diagonal).

438 • At the ultimate post-buckling shear load, almost the entire plate has reached the von
439 Mises yield boundary due to a combination of planar and bending stresses. The
440 contours of von Mises yielding show some differences, however, for the opposing faces
441 of the plate.

442 • Compression membrane stresses (which are independent of the second-order bending
443 effects) continue to increase beyond elastic buckling, contrary to the current tension

444 field theory assumption. These results suggest that compression effects can play a
445 significant role in the post-buckling shear response.

446

447 Building from these results, and with the intent to further investigate the plate behavior,
448 the authors examined some simple modifications of the plate that interrupted the
449 compression diagonal. The results of two cases, with small through-plate cuts removed
450 from the compression diagonal, showed (1) an increase of 10% to 24% in the shear load
451 needed to induce buckling (i.e., the elastic shear buckling load) and (2) a negligible effect
452 on the ultimate shear post-buckling load. These results indicate that the onset of elastic
453 buckling can be delayed by interrupting the compression field, which may prove useful for
454 designing girder webs.

455

456 **Acknowledgments**

457 This research was sponsored by the National Science Foundation (NSF) under grants
458 CMMI-1662886 and CMMI-1662964. Mr. Alós-Moya's involvement in this project as a
459 Visiting Student Research Scholar at Princeton University was financially supported by the
460 Spanish Ministry of Science and Innovation (research project BIA 2011-27104) and the
461 Universitat Politècnica de València (Research and Development Support Program PAID-06-
462 11). All opinions expressed in this paper are the authors' and do not necessarily reflect the
463 policies and views of the sponsors.

Pre-Print Copy: Garlock et al. (2019). "Post-buckling mechanics of a square slender steel plate in pure shear." *Engineering Journal (AISC)*, Vol. 56, No. 1, pp. 27-46.

464 **References**

- 465 AISC (2016). "Specification for Structural Steel Buildings", American Institute of Steel
466 Construction, Chicago, IL.
- 467 Basler, K. "Strength of Plate Girders in Shear," *Trans. ASCE*, vol. 128, no. 2, 1961.
- 468 Basler, K. , Yen, B. T. and Mueller, J. A. (1960). "Web Buckling Tests on Welded Plate
469 Girders," Welding Research Council, Bulletin No. 64 Sept., New York.
- 470 Bergfelt, A. and Hovik, J. (1968). "Thin-walled deep plate girders under static loads," in
471 Proceedings of the IABSE Colloquium, New York.
- 472 Dassault Systemes. (2011). "Abaqus 6.11ef Online Documentation" [Online]. [Accessed
473 2017].
- 474 Evans, H. R. , Rockey, K. C. and Porter, D. M. (1977). "Tests on longitudinally reinforced
475 plate girders subjected to shear," in Proceedings of Conference on Structural Stability,
476 Liege.
- 477 FHWA (1982). Federal Highway Administration, "Standard Plans for Highway Bridges,
478 Volume II, Structural Steel Superstructures."
- 479 Glassman, J., and Garlock, M. (2016). "A Compression Model for Ultimate Post-buckling
480 Shear Strength". *Thin-Walled Structures*, vol. 102, pp. 258–272.
- 481 Garlock, M. E. M. and Glassman, J. D. (2014). "Elevated temperature evaluation of an
482 existing analytical model for steel web shear buckling," *Journal of Constructional Steel*
483 *Research*, vol. 101, pp. 395-406 . doi:10.1016/j.jcsr.2014.05.021.
- 484 Höglund, T. (1997). "Shear Buckling Resistance of Steel and Aluminum Plate Girders,"
485 *Thin-Walled Structures*, vol. 29, pp. 13-30, 1997.

Pre-Print Copy: Garlock et al. (2019). "Post-buckling mechanics of a square slender steel plate in pure shear." *Engineering Journal* (AISC), Vol. 56, No. 1, pp. 27-46.

- 486 Jha, A. (2016). "Investigation of the Shear-Strength of Built-Up I-Section Members Via Test
487 Simulation", A Masters Thesis Presented to the Academic Faculty, Department of Civil
488 and Environmental Engineering, Georgia Institute of Technology.
- 489 Kamtekar, A. G. , J. B. Dwight, J. B. and Threlfall, B. D. (1972). "Tests on Hybrid Plate Girders
490 (Report 2), Report No. CUED/C-Struct/TR28," Cambridge University, Cambridge.
- 491 Narayanan, R. and Rockey, K. C. (1981). "Ultimate load capacity of plate girders with webs
492 containing circular cut-outs," *Proceedings of the Institution of Civil Engineers, Part 2,*
493 *vol. 71, pp. 845-862.*
- 494 Porter, D.M., Rockey, K. C. and Evans, H. R. (1975). "The Collapse Behavior of Plate Girders
495 Loaded in Shear," *Struct. Eng.,* vol. 53, no. 8, pp. 313-325, 1975.
- 496 Rockey, K. C. and Skaloud, M. (1972). "The ultimate load behaviour of plate girders loaded
497 in shear," *The Structural Engineer,* vol. 50, no. 1, pp. 29-48.
- 498 Sakai, F. , Fujii, T. and Fukuchi, Y. (1966). "Failure Tests of Plate Girders Using Large-sided
499 Models," University of Tokyo, Department of Civil Engineering, Structural Engineering
500 Report, Tokyo, 1966.
- 501 Timoshenko, S. P. and Gere, J. M. (1961). *Theory of Elastic Stability*, Second Edition, New
502 York: McGraw-Hill Book Company, Inc.
- 503 Wagner, H. (1931). "Flat Sheet Metal Girder with Very Thin Metal Web", Tech. Notes. 604,
504 605, 606," National Advisory Committee on Aeronautics, Washington, DC.
- 505 White D. W. and Barker M. G. (2008) "Shear Resistance of Transversely Stiffened Steel I-
506 Girders," *Journal of Structural Engineering,* vol. 134, no. 9, pp. 1425-1436.
- 507 Wilson, J. M. (1886). "On Specifications for Strength of Iron Bridges," *Trans. ASCE,* vol. 15,
508 no. Part I, pp. 401-403, 489-490.

Pre-Print Copy: Garlock et al. (2019). "Post-buckling mechanics of a square slender steel plate in pure shear." *Engineering Journal (AISC)*, Vol. 56, No. 1, pp. 27-46.

- 509 Yoo, C. H. and Lee, S. C. (2006). "Mechanics of Web Panel Post-buckling Behavior in Shear,"
510 *Journal of Structural Engineering*, vol. 132, no. 1, pp. 1580-1589.
- 511 Ziemian, R. D. (2010). *Guide to Stability Design Criteria for Metal Structures*, 6th ed.,
512 Hoboken: John Wiley & Sons.